A comprehensive insight into the lipid composition of *Myxococcus xanthus* by UPLC-ESI-MS[S]

Wolfram Lorenzen,* Kenan A. J. Bozhüyük,* Niña S. Cortina,[†,§] and Helge B. Bode[1,*,§]

Merck Stiftungsprofessur für Molekulare Biotechnologie, Fachbereich Biowissenschaften,* Cluster of Excellence Macromolecular Complexes,[†] Buchmann Institute for Molecular Life Sciences (BMLS),[§] Johann Wolfgang Goethe-Universität Frankfurt, D-60438 Frankfurt am Main, Germany

Abstract   Analysis of whole cell lipid extracts of bacteria by means of ultra-performance (UP)LC-MS allows a comprehensive determination of the lipid molecular species present in the respective organism. The data allow conclusions on its metabolic potential as well as the creation of lipid profiles, which visualize the organism's response to changes in internal and external conditions.[JLR] Herein, we describe: *i*) a fast reversed phase UPLC-ESI-MS method suitable for detection and determination of individual lipids from whole cell lipid extracts of all polarities ranging from monoacylglycerophosphoethanolamines to TGs; *ii*) the first overview of a wide range of lipid molecular species in vegetative *Myxococcus xanthus* DK1622 cells; *iii*) changes in their relative composition in selected mutants impaired in the biosynthesis of α-hydroxylated FAs, sphingolipids, and ether lipids; and *iv*) the first report of ceramide phosphoinositols in *M. xanthus*, a lipid species previously found only in eukaryotes.—Lorenzen, W., K. A. J. Bozhüyük, N. S. Cortina, and H. B. Bode. **A comprehensive insight into the lipid composition of *Myxococcus xanthus* by UPLC-ESI-MS.** *J. Lipid Res.* **2014.** 55: 2620–2633.

Supplementary key words   lipidomics • myxobacteria • ceramide phosphoinositols • ether lipids • lipid profiles • electrospray ionization-mass spectrometry • reversed phase • ultra-performance liquid chromatography

Myxobacteria are a globally occurring order of soil-dwelling Gram-negative δ-proteobacteria that attracts interest due to a wide range of remarkable features including cooperative motility, predation, simple multicellularity [including fungi-like fruiting body formation (1)], and as producers of a wide range of secondary metabolites (2). Additionally, they exhibit a complex pattern of primary metabolites, with fatty acyl species and associated lipids the most well-studied. Some of these lipids are involved in processes like chemotaxis or starvation-induced fruiting body formation, either as biomarkers or chemotactic signals (3–5). However, to date, no methodology has been described

that allows researchers to investigate the lipid repertoire of these bacteria as a whole, in order to unveil alterations in the lipid composition on the molecular level as a function of different metabolic conditions or growth stages.

In recent years, progress has been made in elucidating the biosynthesis and putative biological importance of myxobacterial FAs including branched-chain (6), straight-chain (7), unsaturated (8), and hydroxylated FAs, as well as sphingoid species (9), particularly with regard to the best studied myxobacterial model organism *Myxococcus xanthus*. In these studies, methanolysis-derived FA methyl esters (FAMEs) or selected lipid classes were analyzed by means of GC-MS; there is thus only limited information about the complete lipidome of *M. xanthus*. High temperature GC-MS was applied to unhydrolyzed lipid extracts in order to elucidate the structures and relative abundance of neutral lipids (10) and unusual iso-branched alkyldiacylglycerols (4), molecules that exhibit signaling functions in this organism (5). HPLC ESI-MS/MS experiments were used to determine changes in the glycerophosphoethanolamine (PE) composition of mutant strains with inactivated acyltransferases (11) on the one hand, and to determine the ratio of certain ether PEs to acyl PEs during the process of starvation-induced fruiting body formation (4) on the other hand. In a recent publication on the myxobacterial ether lipid biosynthesis and the importance of these lipids for the myxobacterial life cycle (12), all these methods had to be combined in order to examine the effects of gene inactivations on the lipid composition of the respective mutants, as the occurrence and abundance of

Abbreviations: ACN, acetonitrile; AUC, area under the curve; AUR1, inositol phosphorylceramide synthase catalytic subunit; CL, cardiolipin (glycerophosphoglycerophosphoglycerol); DCM, dichloromethane; DG, diacylglycerol; EIC, extracted ion chromatogram; FAME, FA methyl ester; H_2O, water; MeOH, methanol; MG, monoacylglycerol; PA, phosphatidic acid; PE, glycerophosphoethanolamine; PE(P), 1Z-alkenylglycerophosphoethanolamine; PG, glycerophosphoglycerol; PI, glycerophosphoinositol; PI-Cer, ceramide phosphoinositol; PS, phosphatidylserine; RP, reversed phase; UPLC, ultra-performance LC.

[1] To whom correspondence should be addressed:
  e-mail: h.bode@bio.uni-frankfurt.de

[S] The online version of this article (available at http://www.jlr.org) contains supplementary data in the form of eight figures and two tables.

monoacylglycerophosphoethanolamines and ether lipids, as well as glycerolipids, needed to be monitored (12). The availability of a single analytical method, able to detect all lipid species, will facilitate rapid analogous investigations.

Results from TLC resolved $^{32}PO_4^{3-}$ metabolic labeling studies available for *Stigmatella aurantiaca* (13), *Myxococcus fulvus* (14), and *M. xanthus* (15) provide some information about the nature and molar ratio of phosphate-containing lipids present in those strains. However, there is as yet no comprehensive information on the complete lipidome of myxobacteria. This is a prerequisite to visualize and evaluate the changes in lipid composition of mutant strains during vegetative growth or fruiting body formation, as well as providing a basis for further investigations on lipid biomarkers or signals for fruiting body formation.

We sought to develop a LC-MS method that: *i*) is able to resolve as many lipid species as possible, covering lysophospholipids, glycerophospholipids, and glycerolipids; *ii*) gives MS and MS^2 spectra for most of the molecular species in a single run for structure elucidation and identification; *iii*) involves the standard setup of ultra-performance (UP)LC-MS instrumentation used for routine analysis; *iv*) solely uses readily available software; and *v*) needs only a very short measuring time.

Many lipidomic methods that involve the direct measurement of lipid species from lipid extracts are based on direct infusion into ESI sources or ionization by MALDI (16, 17), in which the detection of less abundant molecular species is typically impeded by ion suppression. This effect can be circumvented by separation of the analytes using chromatography (18). The development of a comprehensive LC method for lipids is challenging due to their highly diverse physical properties, ranging from partly water (H_2O) soluble (lysophospholipids) over amphiphilic (glycerophospholipids) to highly nonpolar (glycerolipids), nonionic [glycerolipids, ceramides (Cers)], and strongly pH dependent zwitter, cationic, and anionic molecules (glycerophospholipids). All chromatographic parameters (different eluents, nature, and concentration of additives, as well as temperature and pH) have to be carefully controlled over the whole chromatographic process. The use of eluent additives is limited, as they have to be compatible with MS coupling.

To date, many LC methods have been introduced that involve normal phase chromatography, hydrophilic/lipophilic interaction chromatography, and reversed phase (RP) chromatography, in most cases to address particular analytical challenges (19–21). RP chromatography, which can be regarded as "the" gold standard in routine small molecule analytics, is ideal for resolving molecules with even small differences in polarity, and it is also our method of choice, not least because it is part of our system's standard instrumentation.

EXPERIMENTAL

Materials, chemicals, and analytical standards

H_2O, methanol (MeOH), acetonitrile (ACN), and dichloromethane (DCM) (all Carl Roth) used as solvents and eluents

were of LC-MS grade. HPLC grade ammonia (Sigma) was used as a 10% aqueous solution and formic and acetic acid (both Carl Roth) were of analytical grade. Glyceryl tristearate ~99% {TG(18:0/18:0/18:0); $[M+NH_4]^+ = 908$}, *rac*-1,2-distearoylglycerol ~99% (GC) {diacylglycerol (DG)(18:0/18:0/0:0); $[M+NH_4]^+ = 642$}, 1-stearoyl-*rac*-glycerol ≥99% {monoacylglycerol (MG)(18:0/0:0/0:0); $[M+H]^+ = 359$}, 1,2-dipalmitoyl-*sn*-glycero-3-phosphoethanolamine, synthetic >97% {PE(16:0/16:0); $[M-H]^- = 690$}, 1,2-distearoyl-*sn*-glycero-3-phospho-*rac*-(1-glycerol) sodium salt {glycerophosphoglycerol (PG)(18:0/18:0); $[M-H]^- = 777$}, 1,2-dihexadecyl-*sn*-glycero-3-phosphoethanolamine ≥99.0% (TLC) {PE(*O*-16:0/*O*-16:0); $[M-H]^- = 663$}, 1,2-dipalmitoyl-*sn*-glycero-3-phosphate sodium salt ≥99% (Sigma) {PA(16:0/16:0); $[M-H]^- = 648$}, oleoyl-L-α-lysophosphatidic acid {PA(18:1/0:0); $[M-H]^- = 436$}, 3-*sn*-lysophosphatidylethanolamine from egg yolk {mainly PE(16:0/0:0); $[M-H]^- = 452$ and PE(18:0/0:0); $[M-H]^- = 480$}, Cer from bovine brain >98% (TLC) [mainly Cer(d18:1/18:1)], L-α-phosphatidylinositol from *Glycine max* {mainly glycerophosphoinositol (PI)(18:1/16:1); $[M-H]^- = 833$}, sphingomyelin from chicken egg yolk ~99% {mainly SM(d18:1/16:0); $[M+H]^+ = 703$}, sphingosine 1-phosphate ≥98% (TLC) {mainly CerP(d18:1/0:0); $[M-H]^- = 378$}, 1,2-diacyl-*sn*-glycero-3-phospho-L-serine from bovine brain >97% (TLC) {mainly PS(18:1/16:0) $[M-H]^- = 788$}, and L-α-phosphatidylcholine from egg yolk, type XVI-E, ≥99% (TLC) {mainly PC(18:1/16:0); $[M-H-HCOO]^- = 805$} 14:0 were obtained from Sigma and glycerophosphoglycerophosphoglycerol [cardiolipin (CL)] (ammonium salt) {CL(1'-[14:0l4:0],3'-[14:0/14:0]); $[M-H]^- = 1,240$} from Avanti Polar Lipids were utilized as analytical standards for the development of the optimal eluent system and to produce reference spectra. Stock solutions with a concentration of 1 mg/ml were prepared of each standard in either DCM:MeOH:H_2O 65:35:8 (v/v/v) for the Cers and phospholipids and ACN:DCM 1:1 (v/v) for the neutral lipids and MeOH/10% NH_3 95:5 (v/v) for the sphingosine 1-phosphate. Stock solutions were diluted to a final concentration of 50 μM in MeOH:DCM:H_2O 35:70:5 (v/v/v) prior to HPLC-MS analysis. However, qualitative standards (those that contain a mixture of molecular species) were only diluted 10-fold in MeOH:DCM:H_2O 35:70:5 (v/v/v) prior to HPLC-MS analysis.

Strains and growth conditions

M. xanthus DK1622 wild-type and mutant strains were grown in 150 ml CTT media [10 g Casitone (Difco), 8 mM MgSO$_4$, 1 mM K$_2$HPO$_4$, 10 mM Tris-HCl (pH 7.6)] supplemented with 40 μg/ml kanamycin when appropriate at 30°C and 230 rpm on a rotary shaker in 1 l conical flasks to an optical density of OD$_{600}$ ~1.6. Strains Δ0191, ⁻MXAN_3748, and ⁻MXAN_1528 are published elsewhere (9, 12).

Extraction procedures

Cells were harvested by centrifugation at 15,000 *g* for 15 min at room temperature and washed once with the same volume of distilled H_2O.

A modified method of Bligh and Dyer (22) was applied to extract all lipids. The cell pellets were thoroughly resuspended in 2 ml of distilled H_2O and 7.5 ml of a mixture of MeOH/DCM 2:1 (v/v) was added. After incubation for 20 min under agitation, phase separation was induced by the addition of 2.5 ml of DCM and H_2O, respectively. The lower phase was removed after centrifugation at 750 *g* for 20 min and the cells and upper phase was re-extracted twice with 2 ml DCM. The combined lower phases were filtered through solvent-resistant 0.22 μM polytetrafluoroethylene membrane filters and dried under a stream of nitrogen at 40°C in weighted vials for the exact determination of the mass of the extracts. For analysis, the lipid extracts were dissolved in a

TABLE 1. Identified molecular species with relative AUCs

Compound Name	MM (Da)	Chemical Formula	Molecular Species	m/z (calculated)	Relative Abundance (wild-type)	Relative Abundance Δ0191	Relative Abundance ⁻MXAN_3748	Relative Abundance ⁻MXAN_1528
Cer(d19:0/16:0)	553.5434	C35H71NO3	[M+HCOO]⁻	598.5916	0.9	6.6	0.0	2.6
Cer(d19:0/i17:0 2-OH)	583.5540	C36H73NO4	[M+HCOO]⁻	628.6022	2.9	0.0	0.0	8.6
Cer(d19:0/i17:0)	567.5590	C36H73NO3	[M+HCOO]⁻	612.6072	3.9	22.7	0.0	11.1
Cer-PI(d19:0/16:0 2-OH)	811.5575	C41H82NO12P	[M-H]⁻	810.6002	3.0	0.0	0.0	3.7
Cer-PI(d19:0/16:0)	795.5625	C41H82NO11P	[M-H]⁻	794.6052	1.1	5.8	0.0	1.1
Cer-PI(d19:0/i17:0 2-OH)	825.5731	C42H84NO12P	[M-H]⁻	824.6158	9.9	0.0	0.0	12.3
Cer-PI(d19:0/i17:0)	809.5782	C42H84NO11P	[M-H]⁻	808.6209	4.4	25.1	0.0	4.6
PE(12:1/17:1); PE(13:1/16:1); PE(16:2/13:0); PE(14:1/15:1)	645.4370	C34H64NO8P	[M-H]⁻	644.4797	19.2	18.7	18.3	17.6
PE(14:0/14:0); PE(13:0/15:0)	635.4526	C33H66NO8P	[M-H]⁻	634.4953	5.2	4.7	3.6	3.8
PE(14:0/15:0)	649.4683	C34H68NO8P	[M-H]⁻	648.5110	28.3	26.7	23.1	19.8
PE(14:1/14:1); PE(16:1/12:1); PE(15:1/13:1)	631.4213	C33H62NO8P	[M-H]⁻	630.4640	2.7	3.6	3.5	3.0
PE(14:1/15:0); PE(16:1/13:0)	647.4526	C34H66NO8P	[M-H]⁻	646.4953	50.1	42.6	39.4	38.0
PE(15:0/15:0)	663.4839	C35H70NO8P	[M-H]⁻	662.5266	157.8	128.0	124.9	100.6
PE(15:0/17:0)	691.5152	C37H74NO8P	[M-H]⁻	690.5579	24.8	58.2	25.6	46.7
PE(15:1/13:0)	633.4370	C33H64NO8P	[M-H]⁻	632.4797	6.3	5.5	5.5	5.8
PE(15:1/15:0)	661.4683	C35H68NO8P	[M-H]⁻	660.5110	59.8	41.0	42.5	46.2
PE(16:0/15:0); PE(14:0/17:0)	677.4996	C36H72NO8P	[M-H]⁻	676.5423	6.6	11.8	5.6	10.2
PE(16:0/17:0)	705.5309	C38H76NO8P	[M-H]⁻	704.5736	1.7	2.3	4.1	6.1
PE(16:1/15:0)	675.4839	C36H70NO8P	[M-H]⁻	674.5266	39.3	43.3	37.0	52.7
PE(16:1/15:1); PE(17:1/14:1)	673.4683	C36H68NO8P	[M-H]⁻	672.5110	50.7	43.9	41.7	56.7
PE(16:1/16:1); PE(17:2/15:0)	687.4839	C37H70NO8P	[M-H]⁻	686.5266	47.4	47.5	46.0	57.9
PE(16:1/17:0)	703.5152	C38H74NO8P	[M-H]⁻	702.5579	16.4	21.0	25.5	35.5
PE(16:2/14:1); PE(15:2/15:1)	657.4370	C35H64NO8P	[M-H]⁻	656.4797	13.2	16.0	14.3	12.0
PE(16:2/15:1); PE(15:2/16:1); PE(17:2/14:1)	671.4526	C36H66NO8P	[M-H]⁻	670.4953	26.2	20.9	25.7	24.6
PE(16:2/15:2); PE(17:2/14:2)	669.4370	C36H64NO8P	[M-H]⁻	668.4797	3.3	3.7	4.6	4.1
PE(16:2/16:1); PE(17:2/15:1)	685.4683	C37H68NO8P	[M-H]⁻	684.5110	37.7	4.2	36.1	52.4
PE(17:0/17:0)	719.5465	C39H78NO8P	[M-H]⁻	718.5892	4.7	5.6	16.4	12.7
PE(17:1/15:0); PE(16:1/16:0); PE(15:1/17:0)	689.4996	C37H72NO8P	[M-H]⁻	688.5423	22.2	13.5	26.3	30.9
PE(17:1/16:1)	701.4996	C38H72NO8P	[M-H]⁻	700.5423	10.6	12.7	14.5	14.2
PE(17:1/17:0)	717.5309	C39H76NO8P	[M-H]⁻	716.5736	10.0	10.1	26.5	24.6
PE(17:2/13:0); PE(16:1/14:1); PE(15:1/15:1)	659.4526	C35H66NO8P	[M-H]⁻	658.4953	30.7	26.8	12.8	29.6
PE(17:2/15:2); PE(16:2/16:2)	683.4526	C37H66NO8P	[M-H]⁻	682.4953	23.9	24.8	23.3	23.3
PE(17:2/16:1); PE(16:2/17:1)	699.4839	C38H70NO8P	[M-H]⁻	698.5266	31.9	29.3	38.6	36.6
PE(17:2/16:2)	697.4683	C38H68NO8P	[M-H]⁻	696.5110	21.8	20.3	25.4	22.1
PE(17:2/17:0); PE(17:1/17:1)	715.5152	C39H74NO8P	[M-H]⁻	714.5579	10.4	8.6	19.6	18.0
PE(17:2/17:1)	713.4996	C39H72NO8P	[M-H]⁻	712.5423	10.5	7.5	17.2	11.6
PE(17:2/17:2)	711.4839	C39H70NO8P	[M-H]⁻	710.5266	5.4	4.3	9.7	6.5
PE(P-15:0/15:0)	647.4890	C35H70NO7P	[M-H]⁻	646.5317	98.3	115.0	126.3	6.5
PE(P-15:0/17:0)	675.5203	C37H74NO7P	[M-H]⁻	674.5630	3.1	2.3	6.7	0.0
PG(14:0/15:0)	680.4628	C35H69O10P	[M-H]⁻	679.5055	3.4	5.4	3.9	3.6
PG(15:0/15:0)	694.4785	C36H71O10P	[M-H]⁻	693.5212	15.4	21.6	16.1	13.6
PG(15:0/15:1); PG(16:1/14:0)	692.4628	C36H69O10P	[M-H]⁻	691.5055	4.2	5.2	3.9	5.1
PG(15:0/16:1); PG(14:1/17:0)	706.4785	C37H71O10P	[M-H]⁻	705.5212	6.2	9.2	7.1	10.1
PG(15:1/16:1); PG(15:0/16:2); PG(14:1/17:1); PG(14:0/17:2)	704.4628	C37H69O10P	[M-H]⁻	703.5055	3.0	4.3	3.2	2.9
PG(16:0/16:1); PG(15:1/17:0); PG(15:0/17:1)	720.4941	C38H73O10P	[M-H]⁻	719.5368	5.2	7.9	6.4	8.5
PG(16:0/17:0)	736.5254	C39H77O10P	[M-H]⁻	735.5681	1.0	2.7	3.2	3.1
PG(16:1/16:1)	718.4785	C38H73O10P	[M-H]⁻	717.5212	3.4	11.3	7.3	15.3
PG(16:1/16:2)	716.4628	C38H69O10P	[M-H]⁻	715.5055	1.6	2.4	1.9	4.3
PG(17:0/16:1)	734.5098	C39H75O10P	[M-H]⁻	733.5525	6.8	13.1	15.1	14.6
PG(17:0/17:0)	750.5411	C40H79O10P	[M-H]⁻	749.5838	2.1	3.1	16.4	4.4
PG(17:0/17:1)	748.5254	C40H77O10P	[M-H]⁻	747.5681	2.7	4.6	6.7	4.1
PG(17:1/16:1)	732.4941	C39H73O10P	[M-H]⁻	731.5368	3.6	4.7	8.4	9.0
CL(60:0)	1296.9096	C69H134O17P2	[M-H]⁻	1295.9024	1.8	0.9	0.4	0.6
CL(60:1)	1294.8940	C69H132O17P2	[M-H]⁻	1293.8867	1.8	0.9	0.4	0.8
CL(60:2)	1292.8783	C69H130O17P2	[M-H]⁻	1291.8711	1.3	0.6	0.3	0.7
CL(60:3)	1290.8627	C69H128O17P2	[M-H]⁻	1289.8554	0.5	0.3	0.2	0.3
CL(61:1)	1308.9096	C70H134O17P2	[M-H]⁻	1307.9023	2.0	1.1	0.5	1.1
CL(61:2)	1306.8940	C70H132O17P2	[M-H]⁻	1305.8867	2.1	1.1	0.4	1.4
CL(61:3)	1304.8783	C70H130O17P2	[M-H]⁻	1303.8711	1.2	0.7	0.3	0.9
CL(61:4)	1302.8627	C70H128O17P2	[M-H]⁻	1301.8554	0.4	0.3	0.1	0.3
CL(62:0)	1324.9409	C71H138O17P2	[M-H]⁻	1323.9337	0.6	0.3	0.2	0.4
CL(62:1)	1322.9253	C71H136O17P2	[M-H]⁻	1321.9180	1.7	1.1	0.5	0.7

TABLE 1. Continued.

Compound Name	MM (Da)	Chemical Formula	Molecular Species	m/z (calculated)	Relative Abundance (wild-type)	Relative Abundance Δ0191	Relative Abundance ⁻MXAN_3748	Relative Abundance ⁻MXAN_1528
CL(62:2)	1320.9096	C71H134O17P2	[M-H]⁻	1319.9024	2.7	1.6	0.6	1.9
CL(62:3)	1318.8940	C71H132O17P2	[M-H]⁻	1317.8867	1.8	1.1	0.5	1.6
CL(62:4)	1316.8783	C71H130O17P2	[M-H]⁻	1315.8711	0.8	0.5	0.2	0.7
CL(62:5)	1314.8627	C71H128O17P2	[M-H]⁻	1313.8554	0.2	0.2	0.1	0.2
CL(63:0)	1338.9566	C72H140O17P2	[M-H]⁻	1337.9493	0.4	0.3	0.1	0.3
CL(63:1)	1336.9409	C72H138O17P2	[M-H]⁻	1335.9337	1.3	0.9	0.5	1.0
CL(63:2)	1334.9253	C72H136O17P2	[M-H]⁻	1333.9180	2.1	1.1	0.6	1.7
CL(63:3)	1332.9096	C72H134O17P2	[M-H]⁻	1331.9023	2.0	1.1	0.5	1.9
CL(63:4)	1330.8940	C72H132O17P2	[M-H]⁻	1329.8867	1.1	0.7	0.3	1.3
CL(63:5)	1328.8783	C72H130O17P2	[M-H]⁻	1327.8711	0.5	0.3	0.1	0.5
CL(64:0)	1352.9722	C73H142O17P2	[M-H]⁻	1351.9650	0.2	0.1	0.1	0.2
CL(64:1)	1350.9566	C73H140O17P2	[M-H]⁻	1349.9493	0.5	0.3	0.3	0.5
CL(64:2)	1348.9409	C73H138O17P2	[M-H]⁻	1347.9337	1.2	0.7	0.4	1.2
CL(64:3)	1346.9253	C73H136O17P2	[M-H]⁻	1345.9180	1.6	0.9	0.5	1.8
CL(64:4)	1344.9096	C73H134O17P2	[M-H]⁻	1343.9023	1.2	0.8	0.4	1.6
CL(64:5)	1342.8940	C73H132O17P2	[M-H]⁻	1341.8867	0.7	0.5	0.2	0.8
CL(64:6)	1340.8783	C73H130O17P2	[M-H]⁻	1339.8710	0.3	0.2	0.1	0.3
CL(65:1)	1364.9722	C74H142O17P2	[M-H]⁻	1363.9650	0.2	0.2	0.1	0.3
CL(65:2)	1362.9566	C74H140O17P2	[M-H]⁻	1361.9493	0.6	0.2	0.3	0.5
CL(65:3)	1360.9409	C74H138O17P2	[M-H]⁻	1359.9336	1.1	0.7	0.4	1.3
CL(66:1)	1378.9879	C75H144O17P2	[M-H]⁻	1377.9806	0.7	0.1	0.1	0.2
CL(66:2)	1376.9722	C75H142O17P2	[M-H]⁻	1375.9650	0.3	0.2	0.2	0.4
DG(15:0/15:0/0:0)	540.4754	C33H64O5	[M+NH4]⁺	558.5092	16.9	8.2	12.8	6.8
DG(31:1)	552.4754	C34H64O5	[M+NH4]⁺	570.5092	6.4	2.5	3.8	6.1
DG(32:0)	568.5067	C35H68O5	[M+NH4]⁺	586.5405	2.4	2.3	3.0	2.2
DG(32:2)	564.4754	C35H64O5	[M+NH4]⁺	582.5092	6.3	2.3	4.3	4.0
DG(33:0)	582.5223	C36H70O5	[M+NH4]⁺	600.5561	1.0	0.9	1.0	0.9
DG(33:1)	580.5067	C36H68O5	[M+NH4]⁺	598.5405	3.2	2.1	4.0	3.7
DG(33:2)	578.491	C36H66O5	[M+NH4]⁺	596.5248	4.5	0.0	1.6	3.8
TG(15:0/15:0/15:0)	764.6894	C48H92O6	[M+NH4]⁺	782.7232	94.8	111.8	86.6	46.0
TG(38:1)	666.5798	C41H78O6	[M+NH4]⁺	684.6136	1.7	2.9	1.8	2.2
TG(39:0)	680.5955	C42H80O6	[M+NH4]⁺	698.6293	5.5	9.5	7.8	4.9
TG(39:1)	678.5798	C42H78O6	[M+NH4]⁺	696.6136	2.5	4.3	2.4	3.4
TG(40:1)	692.5955	C43H80O6	[M+NH4]⁺	710.6293	6.0	9.4	6.1	6.8
TG(40:2)	690.5798	C43H78O6	[M+NH4]⁺	708.6136	3.2	3.9	2.9	4.4
TG(41:1)	706.61114	C44H82O6	[M+NH4]⁺	724.6450	10.4	13.7	11.4	10.9
TG(41:2)	704.5955	C44H80O6	[M+NH4]⁺	722.6293	5.0	6.8	5.3	6.1
TG(41:3)	702.5798	C44H78O6	[M+NH4]⁺	720.6136	2.1	2.5	1.9	2.6
TG(42:1)	720.62679	C45H84O6	[M+NH4]⁺	738.6606	20.3	25.3	21.1	18.9
TG(42:2)	718.6111	C45H82O6	[M+NH4]⁺	736.6449	15.7	13.7	14.1	15.2
TG(43:0)	736.6581	C46H88O6	[M+NH4]⁺	754.6919	33.3	44.1	35.6	17.6
TG(43:1)	734.6424	C46H86O6	[M+NH4]⁺	752.6762	23.9	25.5	23.1	18.7
TG(43:2)	732.6268	C46H84O6	[M+NH4]⁺	750.6606	22.2	22.3	19.7	22.2
TG(43:3)	730.6111	C46H82O6	[M+NH4]⁺	748.6449	9.4	8.1	6.7	9.3
TG(44:0)	750.6737	C47H90O6	[M+NH4]⁺	768.7075	35.6	25.0	38.2	19.5
TG(44:1)	748.6581	C47H88O6	[M+NH4]⁺	766.6919	40.6	45.5	36.7	32.8
TG(44:2)	746.6424	C47H86O6	[M+NH4]⁺	764.6762	32.4	27.4	24.7	28.1
TG(44:3)	744.6268	C47H84O6	[M+NH4]⁺	762.6606	18.4	11.5	11.1	16.2
TG(44:4)	742.6111	C47H82O6	[M+NH4]⁺	760.6449	4.2	3.8	2.5	4.4
TG(45:1)	762.6737	C48H90O6	[M+NH4]⁺	780.7075	49.9	45.0	41.4	41.2
TG(45:2)	760.6581	C48H88O6	[M+NH4]⁺	778.6919	34.7	32.1	29.8	37.4
TG(45:3)	758.6424	C48H86O6	[M+NH4]⁺	776.6762	25.0	18.8	16.9	27.1
TG(45:4)	756.62679	C48H84O6	[M+NH4]⁺	774.6606	9.3	6.6	5.5	10.0
TG(46:0)	778.70504	C49H94O6	[M+NH4]⁺	796.7389	37.3	43.9	34.6	24.7
TG(46:1)	776.6894	C49H92O6	[M+NH4]⁺	794.7232	52.6	56.3	49.8	57.7
TG(46:2)	774.6737	C49H90O6	[M+NH4]⁺	792.7075	45.4	43.2	39.5	51.9
TG(46:3)	772.6581	C49H88O6	[M+NH4]⁺	790.6919	27.3	18.9	20.8	29.2
TG(47:0)	792.7207	C50H96O6	[M+NH4]⁺	810.7545	48.8	59.8	62.0	41.1
TG(47:1)	790.705	C50H94O6	[M+NH4]⁺	808.7388	36.2	33.6	41.7	46.0
TG(47:2)	788.68939	C50H92O6	[M+NH4]⁺	806.7232	33.4	32.2	33.4	50.9
TG(47:3)	786.6737	C50H90O6	[M+NH4]⁺	804.7075	21.0	17.5	18.0	9.7
TG(47:4)	784.6581	C50H88O6	[M+NH4]⁺	802.6919	13.1	8.7	8.9	21.0
TG(48:0)	806.7363	C51H98O6	[M+NH4]⁺	824.7701	15.7	18.2	24.4	21.4
TG(48:1)	804.72069	C51H96O6	[M+NH4]⁺	822.7545	21.0	27.6	30.5	36.8
TG(48:2)	802.705	C51H94O6	[M+NH4]⁺	820.7388	17.9	19.2	23.7	36.0
TG(48:3)	800.6894	C51H92O6	[M+NH4]⁺	818.7232	17.8	12.7	15.4	26.5
TG(48:4)	798.6737	C51H90O6	[M+NH4]⁺	816.7075	10.1	7.6	9.8	17.0
TG(49:0)	820.752	C52H100O6	[M+NH4]⁺	838.7858	14.8	20.1	30.0	19.7
TG(49:1)	818.7363	C52H98O6	[M+NH4]⁺	836.7701	12.0	12.4	20.7	21.7
TG(49:2)	816.7207	C52H96O6	[M+NH4]⁺	834.7545	11.1	11.2	17.2	24.0
TG(50:0)	834.7676	C53H102O6	[M+NH4]⁺	852.8014	4.5	5.5	8.9	8.2

TABLE 1. Continued.

Compound Name	MM (Da)	Chemical Formula	Molecular Species	m/z (calculated)	Relative Abundance (wild-type)	Relative Abundance Δ0191	Relative Abundance ‾MXAN_3748	Relative Abundance ‾MXAN_1528
TG(50:1)	832.752	C53H100O6	$[M+NH_4]^+$	850.7858	6.0	6.8	11.5	12.6
TG(51:0)	848.7833	C54H104O6	$[M+NH_4]^+$	866.8171	3.0	3.8	9.0	4.9
TG(51:1)	846.7676	C54H102O6	$[M+NH_4]^+$	864.8014	3.0	2.8	5.6	5.1
TG(52:0)	862.7989	C55H106O6	$[M+NH_4]^+$	880.8327	1.1	0.5	0.8	0.9

Relative AUCs given as per thousand of the total AUC of all identified lipid molecular species determined separately for positive and negative ionization modes. MM (molecular mass) is the calculated molecular weight of monoisotopic mass of respective lipid species. See supplementary Tables I, II for details.

mixture of MeOH:DCM:H_2O (35:70:5, v/v/v) to a final concentration of 10 mg/ml.

GC-MS FAME analysis

Derivatization procedures and GC-MS conditions are described elsewhere (23).

HPLC-MS conditions

For every data set, 5 µl of lipid extract was separated on an ACQUITY UPLC™ BEH C18 column (Waters) with a length of 50 mm, an inner diameter of 2.1 mm, and a mean particle size of 1.7 µM connected to an UltiMate 3000 (Thermo) HPLC system coupled to an AmaZon X (Bruker) mass spectrometer at a constant flow rate of 0.6 ml/min and a temperature of 50°C using a binary gradient. Eluent A consisted of H_2O/ACN 50/50 (v/v) and solvent system B of ACN/isopropanol 10/90 (v/v). Both eluents contained 10 mM NH_4AcO as a buffering additive and were adjusted to pH 5.5 using formic acid in order to maintain the analytes in the same charge state during the separation process. The gradient was programmed as follows: start at 1% B, increased to 95% within 10 min in a linear manner, hold at 95% for 2 min and re-equilibrate for 2 min at 1% B.

The ESI parameters for the negative ion mode were: capillary voltage, +4.5 kV (negative mode) −4.5 kV (positive mode); end plate offset, −500 V; capillary exit, −140 V (negative mode)

+140 V (positive mode); nitrogen flow, 11.83 l/min; drying gas temperature, 300°C; and nebulizing gas pressure, 44 psi.

Both MS and MS/MS data were recorded in the same run using the "ultra" scan mode with a trap drive of 64.3 (negative mode) and 53.3 (positive mode), respectively, a scan speed of m/z 25,000 per second and a mass resolution of m/z 0.6 over a range of m/z 100–2,000, with one spectrum having an average of seven scans in the MS mode and three scans in the MS^2 mode. For autoMS/MS fragmentation, an absolute threshold of 25,000 cts was chosen, and already fragmented precursor ions were excluded for further fragmentation after two spectra for 0.5 min. The isolation width was m/z 1.5.

Data processing

For the visualization, processing, and analysis of the HPLC-MS data, the program DataAnalysis version 4.0 SP 2 (Build 274, Bruker) was used in combination with LibraryEditor version 4.0 SP 2 (Build 274, Bruker) and Excel 2010 [version 14.0.7106.5003 (32-bit)].

In a first step, a LibraryEditor library was established to enable automatic identification of lipid species from the lipid extracts. MS^2 spectra that were acquired during the runs were automatically extracted from the data set using the "Compound − autoMS(n)" algorithm with the following settings: intensity threshold positive, 1,000,000; intensity threshold negative, 10,000; maximum number of compounds, 350; retention time window (min), 0.25; spectrum type, line spectra only; background subtraction, none. Lipid species were identified from the MS^2 spectra and added to the library together with their retention times. This library was applied to all HPLC-MS runs using the "Identify Mass Spectra" function of data analysis with the following settings: desired score, 900; minimum score, 600; minimum parameter matching score, 250; maximum number of spectra, 1; accepted retention time deviation, 0.1 min; maximum retention time deviation, 0.2 min.

For the calculation of the relative percent of lipid species, extracted ion chromatograms (EICs) were created for every single precursor ion of the identified lipid species. All chromatographic traces were smoothed using a Gaussian algorithm (1 pt width, 2 cycles) to enhance peak detection. Those EICs from the identified lipid species were integrated by applying the "Compounds − Chromatograms" algorithm with the following settings: signal-to-noise threshold, 5; area threshold, 10%; intensity threshold, 10,000 for the negative ion mode and 1,000,000 for the positive ion mode; skim ratio, 0; smoothing width, 1. Charts containing the identified autoMSn compounds and the areas under the curve (AUCs) of the EICs were exported into Excel charts. Those charts were manually inspected for false identifications and missing EIC peak integrations.

Peak areas of PEs, PGs, Cer phosphoinositols (PI-Cers), the formate adducts of Cers, 1 Z-alkenylglycerophosphoethanolamines
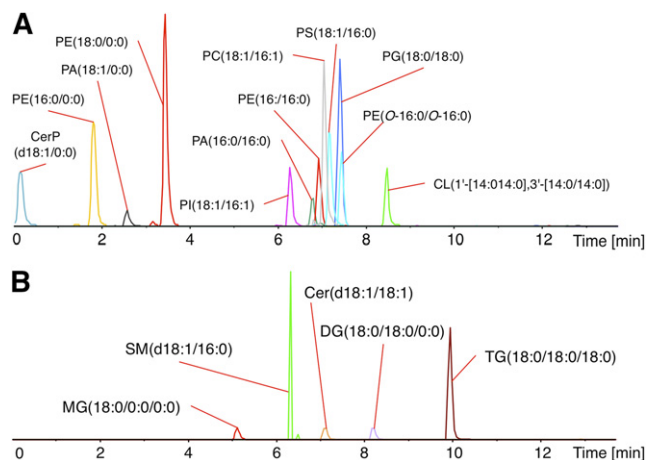

Fig. 1. EICs of lipid standards. Data acquired in negative (A) and positive (B) ionization mode with standards mentioned in the Experimental section. All lipids were resolved by the applied eluent system. For details see the Experimental section. CerP, sphingoid base 1-phosphate; PA, mono/diacylglycerophosphate; PC, glycerophosphocholine; PE(O/O), dialkylglycerophosphoethanolamine; PS, glycerophosphoserine; SM, Cer phosphocholine.
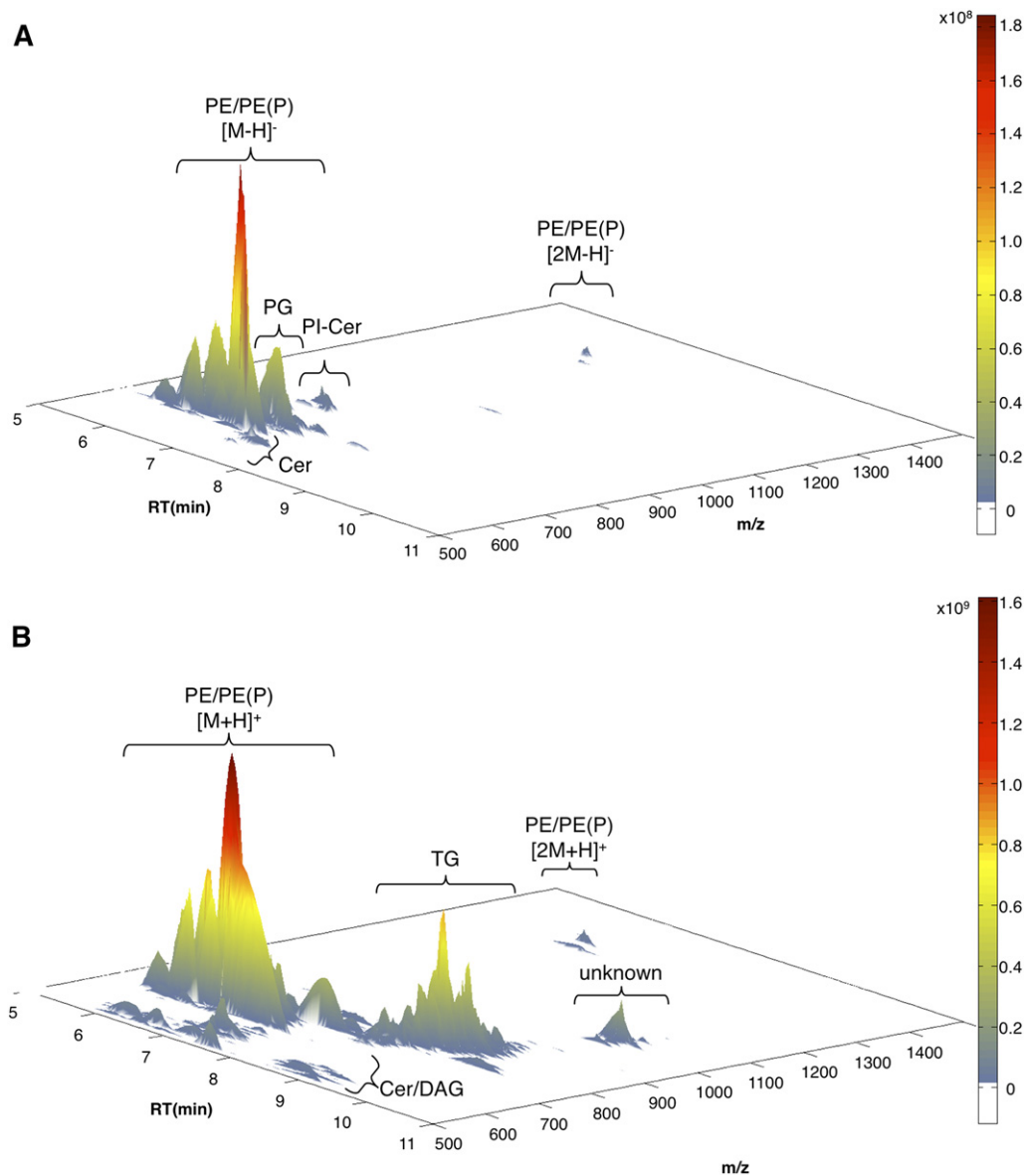
Fig. 2. Base peak UPLC-ESI-MS chromatograms of a DK1622 lipid extract. Data acquired in negative (A) and positive (B) ionization mode. CLs were detected in the negative ionization mode at retention time ∼8–9 min, but their $[M\text{-}H]^-$ ions are of low abundance ($<2 \times 10^5$ counts).

[PE(P)s], and CLs from the HPLC-MS runs in the negative ionization mode and the DGs and TGs in the positive ion mode were separately summed and normalized to 1,000, and the peak area of each individual EIC peak was calculated as per milliliter of the total integral of all peaks (see supplementary Table I and II for the complete data set and **Table 1** for a summary).

MATLAB release 2013b (The MathWorks, Inc., Natick, MA) was used for the visualization of the base peak full scan UPLC-ESI-MS chromatograms and plotting the lipid profiles. The base peak full scan UPLC-ESI-MS chromatograms were created by using the functions "meshgrid" and "surf". The "stem3" function was applied to create the 3D lipid profiles.

Identification of lipids by MS

The experiments of the positive ionization and the negative ionization mode were combined in order to identify a maximum possible number of lipids. The above-mentioned standards were used in order to evaluate the chromatographic and fragmentation behavior of those lipid species. This information plus the reference spectra and software tools from LIPID MAPS (24) were used as the bases for the MS-based structure elucidation of the lipid species. The fragmentation behavior of PI-Cers have been described previously (25, 26). ESI-MS data for the identification and structure elucidation of PGs, PEs, and CLs, as well as glycerolipids (DGs and TGs) are also available (27–32). The presence of PGs, PEs, and *N*-acylsphinganines (Cers), as well as the presence of distinctive α-hydroxylated FAs together with the complete FA profiles of the investigated strains have been published (9, 11, 14, 15).

In negative ion mode, PGs, PEs, and CLs were detected as $[M\text{-}H]^-$ ions, and Cers, both hydroxylated and nonhydroxylated, as $[M+HCOO]^-$ ions, respectively.

PEs, Cers, MGs, DGs, and TGs were detected in the positive ion mode, the former two as $[M+H]^+$ ions and the latter two as $[M+NH_4]^+$ ions (33).

In general, isobaric molecular species could not be resolved by HPLC, and thus yielded one MS^2 spectra (see Tables 1, 3; supplementary Figs. I–VII)

For the creation of the lipid profiles, only the integrals from the negative ion mode for the PEs, PGs, PI-Cers, and Cers and from the positive ion mode for the DGs and TGs were used. PE and Cer ions were also clearly detectable in positive ion mode, but not used for the creation of lipid profiles.

High resolution MS analyses

Determination of the exact mass of Cer molecular species from lipid extracts was carried out using a Dionex Ultimate 3000 RSLC coupled to a Bruker micrOTOF-Q II equipped with an ESI source set to negative ionization mode. HPLC settings were identical to those described above, though the column bed was 100 mm in length and the gradient length was doubled to 20 min accordingly. The mass spectrometer was calibrated using a sodium formate calibrant solution (10 mM). MS data were acquired within the mass range of m/z 200–2,000.

Nomenclature

For the sake of uniformity and comprehensibility, we used the nomenclature of the LIPID MAPS Lipid Classification System (24) for the names and abbreviations.

RESULTS

A binary eluent system consisting of H_2O and ACN in solvent A and ACN and isopropanol in solvent B (for details see the Experimental section) proved to be useful for the separation and elution of an extensive range of lipid standards on a RP-18 column, including glycerolipids, glycerophospholipids, and sphingolipids with different degrees of acylation, as well as acidic, basic, and amphoteric polar head groups (**Fig. 1**). The use of a 10 mM ammonium acetate buffer adjusted with formic acid to pH 5.5, a pH at which all major phospholipids have an equable charge state (34, 35), gave an acceptable separation of the lipid extract of *M. xanthus* DK1622 (36) as depicted in **Fig. 2**, while ESI-MS/MS analysis allowed the detection and identification of eluting lipid species (supplementary Figs. I–VII).

Lipid profile of *M. xanthus*

Applying the described method to normalized lipid extracts resulted in two sets of LC-MS data for each sample: one recorded in the positive ionization mode and the other one in the negative ionization mode. Figure 2 shows
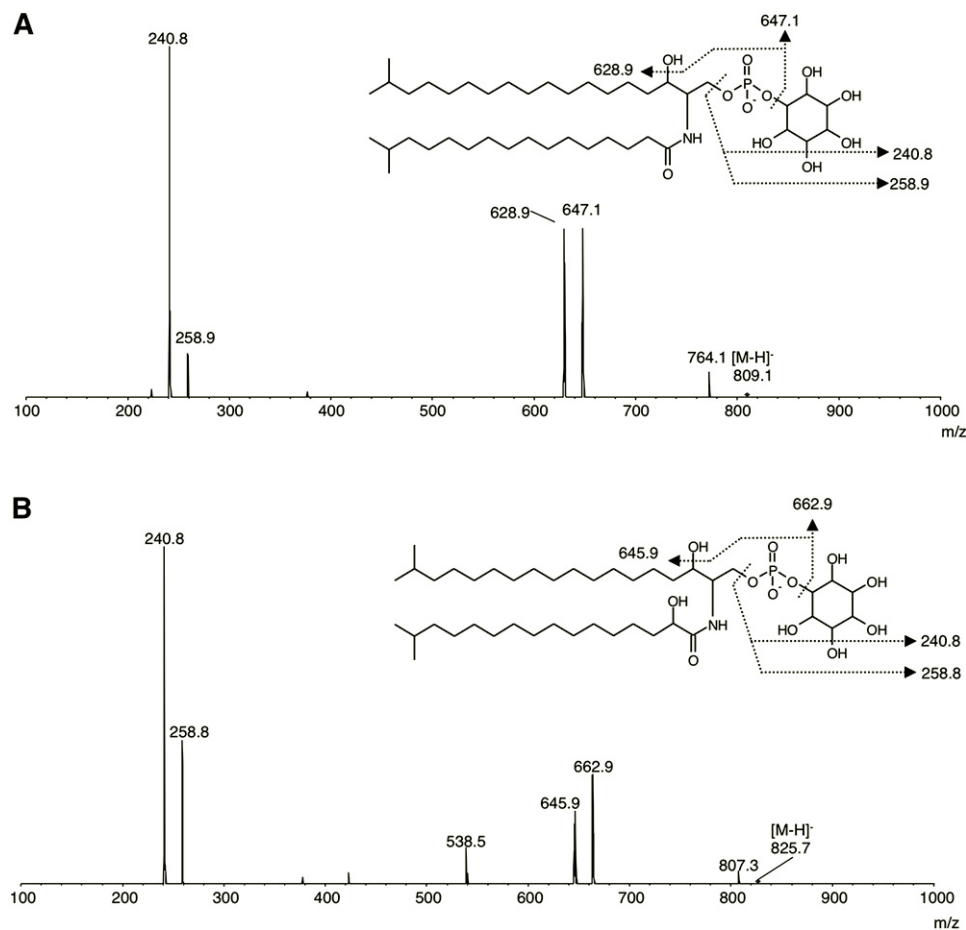

Fig. 3. Example spectra for PI-Cer identification. MS^2 fragment spectra of PI-Cer(d19:0/17:0) (A) and PI-Cer(d19:0/17:0 2-OH) (B). Fragments are [inositol phosphate]$^-$, [inositol phosphate-H$_2$O]$^-$, [P-Cer-H$_2$O]$^-$, and [P-Cer]$^-$ (45, 46). Molecular composition was confirmed by high-resolution MS (see Table 3).

the resulting base peak chromatograms of the LC-MS analysis of lipid extracts from vegetatively grown DK1622 cells in negative (Fig. 2A) and positive (Fig. 2B) ionization modes, respectively.

The most intense signals are discernable in the region of R_t = ~6.0–8.5 min and have m/z values of approximately 550–850 in negative ion mode, with another large group of signals occurring at R_t = ~9.0–10.5 min and having m/z values of 700–880 in positive ionization mode. Additionally, the most intense glycerophospholipid molecular species are discernable as dimeric ions, and there is an unknown compound class with a strong abundance at R_t = ~9.8 min with about m/z 1,008, which could not be identified.

Evaluation of autoMS^2 data resulted in the identification of a large number of PE and PG species, as well as the previously identified PE(P)s (4) (supplementary Figs. I–III), hydroxylated and nonhydroxylated N-acylsphinganines (Cers) (supplementary Fig. IV), and interestingly, for the first time in a prokaryote, PI-Cers [**Fig. 3**; for a summary see Table 1 and supplementary Table I and II (the full data set obtained from data analysis)]. Consistent with the relative low abundance and limited diversity of sphingoid bases, as determined by GC-MS analysis of lipid methanolyzed cell extracts (**Table 2**), they are detectable as less abundant compounds. Finally, CLs are detectable as late eluting compounds with rather low abundances (supplementary Fig. V).

Fragmentation spectra of the late eluting molecules in positive ionization mode are consistent with ammonium adducts of DGs and TGs (37) (supplementary Figs. VI, VII),

as well as protonated Cers. PEs are the only detectable glycerophospholipid species and are distinguished by the $[M-141+H]^+$ MS^2 fragment resulting from the neutral loss of the polar headgroup. They were not further evaluated, as these fragment spectra do not contain any additional structural information.

None of the evaluated MS^2 spectra displayed evidence for other glycerophospholipids, glycerolipids, or precursors of identified lipids such as lysophospholipids, diacylglycerophosphoserines, or PIs.

Concerning the elution pattern of these lipid species, the following regularities can be observed (see Fig. 2; Table 1; supplementary Tables I, II): *i*) As expected, retention time increases with increasing length of the acyl chains attached to the glycerophospholipids, as hydrophobic interaction with the RP-18 stationary phase becomes more intense. *ii*) Elution order for glycerophospholipids is PGs → PEs → PE(P)s → CLs, as long as the number of carbon atoms and the degree of saturation in the acyl side chains are identical. *iii*) PI-Cers elute earlier than Cers, whereas α-hydroxylation in the acyl side chain further decreases the retention time. *iv*) For DGs and TGs, analogously to the glycerophospholipids, retention time increases with acyl chain length and degree of saturation. *v*) Lipids from the same class with an identical overall carbon and double bond number generally coelute. However, data from MS^2 fragmentation of glycerophospholipids in the negative ion mode does allow the assignment of fatty acyl residues to *sn*-1 or *sn*-2 positions of the glycerol backbone of those lipid species (supplementary Figs. I–III).

TABLE 2. Complete FAME-GC-MS data from DK1622 wild-type and mutants in percent of all FAMEs

Fatty acid	Wild-type	Δ0191 (9)	⁻MXAN_3748 (9)	⁻MXAN_1528 (12)
12:0	0.09	<0.17	0.05	0.08
iso-13:0	0.33	0.33	0.25	0.59
iso-14:0	0.16	0.00	<0.05	<0.08
14:1ω9c	1.23	0.49	0.57	0.20
14:1ω3c	0.04	<0.17	0.05	<0.08
14:0	5.85	2.65	3.43	3.05
iso-15:1ω9c	0.32	0.16	0.11	0.29
iso-15:0	38.93	40.67	33.62	33.86
15:0	2.78	0.74	4.06	2.07
15:1ω10c	3.54	1.03	2.89	2.21
15:1ω4c	3.04	0.69	2.92	2.11
iso-16:0	<0.09	<0.17	3.31	<0.08
16:2ω5c,11c	4.92	4.61	4.53	5.33
16:1ω11c	0.97	0.85	1.15	1.17
16:1ω5c	11.48	13.03	14.08	17.45
16:0	1.88	3.29	2.65	1.99
iso-17:2ω5c,11c	1.67	2.84	3.12	2.94
iso-17:1ω11c	0.74	1.00	1.79	1.33
iso-17:1ω5c	1.39	1.80	3.57	2.34
iso-17:0	3.35	9.38	7.88	4.99
14:0 3-OH	0.53	0.13	0.55	0.55
iso-15:0 3-OH	2.88	2.06	3.21	3.32
16:0 2-OH	0.79	<0.17	<0.05	0.87
16:0 3-OH	0.47	<0.17	0.51	0.23
iso-17:0 2-OH	4.67	<0.17	<0.05	10.28
iso-17:0 3-OH	1.16	0.25	1.69	0.13
iso-15:0 DMA	2.42	8.99	4.19	0.08
iso-15:0 OAG	0.87	3.39	3.06	0.15
d18:0	0.68	0.17	<0.05	0.45
iso-d19:0	2.92	1.46	<0.05	1.96

DMA, vinyl ether-derived dimethyl acetals; OAG, ether-derived O-alkylglycerols; d, sphingoid bases.

In total, 3 Cers, 4 PI-Cers, 52 PEs, 2 PE(P)s, 20 PGs, 32 glycerophosphoglycerophosphoglycerols, and 7 DGs were identifiable. Additionally, 46 TG molecular species were identified, but the exact assignment of all three fatty acyl moieties to the three hydroxyl functions of the glycerol backbone was not possible under these conditions, as only MS^3 fragments of the $[M-NH_3-R_nCOOH]^+$ ions allow the assignment of the fatty acyl residues to a particular hydroxy group of the glycerol backbone. Nevertheless, the fragment spectra of TGs indicated a high diversity of those molecules comprising almost all saturated and unsaturated FAs present in *M. xanthus*. Beyond that, all TG ion species consisted of several isobaric TG species which coeluted, just as observed for the PGs and PEs (supplementary Fig. VIIC). We did not test the use of adduct-forming additives such as Li^+ and Na^+ because this would only further increase the number of ionic species and would not solve the problem of overlapping tandem mass spectra; the same applies to the CLs. Only MS^3 experiments allow the exact determination of the acyl residues present in the

$[PA+131]^-$ or $[PG-H_2O]^-$ fragments (30) (supplementary Fig. V).

UPLC-MS analysis allows the assignment of a particular polar headgroup to Cers and detects loss of lipid species in mutant strains

We applied the UPLC-MS method and data evaluation procedure to lipid extracts of vegetatively grown cells from various strains with mutations in different genes involved in lipid biosynthesis. Strain Δ0191 lacks a FA hydroxylase, which is responsible for the formation of 2-OH FAs (Table 2). Strain ⁻MXAN_3748 bears a mutation in a serine-palmitoyl-CoA acyltransferase homolog and is impaired in sphingoid base formation (9) (Table 2). **Figure 4A, B** shows EICs of various Cer species from wild-type, Δ0191, and ⁻MXAN_3748 extracts. Strain Δ0191 shows the selective loss of hydroxylated Cers (Fig. 4A). Strain ⁻MXAN_3748 no longer forms either Cers or PI-Cers, as determined by both low resolution MS and confirmative high resolution MS experiments (Fig. 4B, **Table 3**).
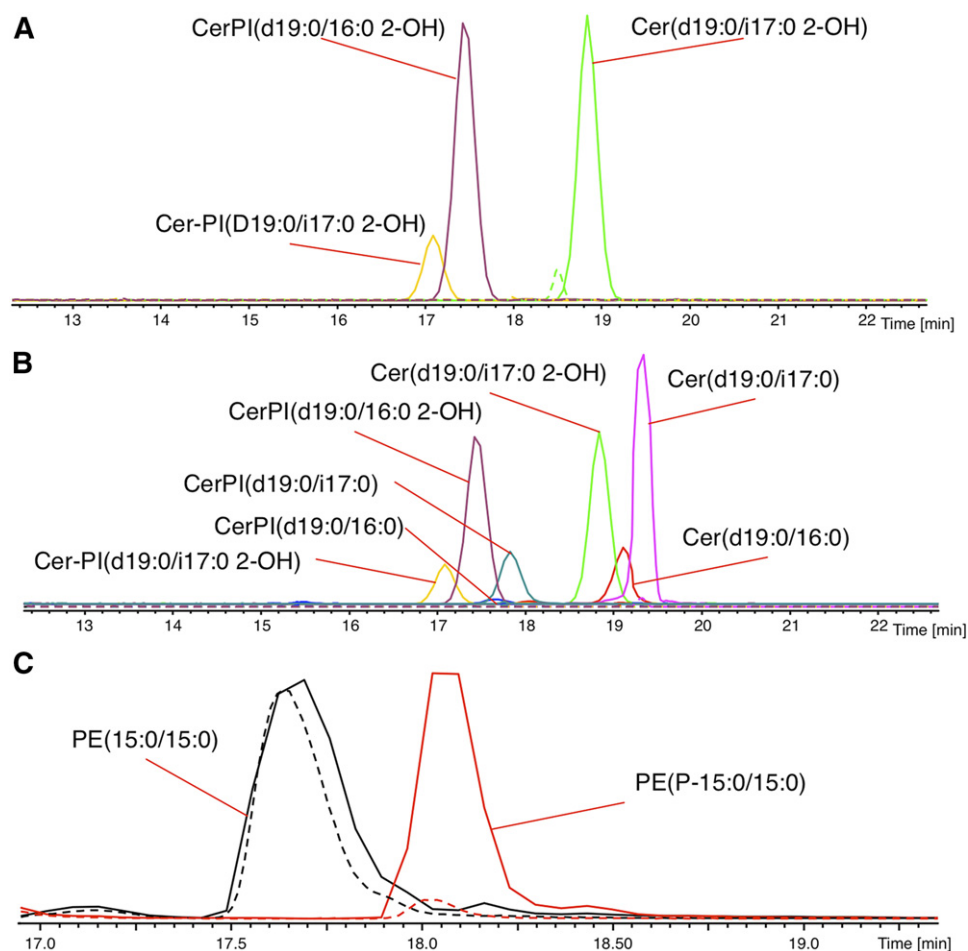

Fig. 4. EICs of *N*-acylsphinganines, PI-Cers, and PE(P)s in wild-type and mutant strain lipid extracts. Solid lines are EICs of the indicated molecular species from *M. xanthus* wild-type, dotted lines from strains Δ0191 (A), ⁻MXAN_3748 (B), and ⁻MXAN_1528 (C), respectively, showing the loss of hydroxylated sphingolipids (A), sphingolipids in general (B), and PE(P)s (C). Intensity scale is normalized to 2.5×10^4 (A), 1.5×10^4 (B), and 1.5×10^5 (C) counts. Chromatograms are taken from HPLC-high resolution MS readings (see the Experimental section).

TABLE 3. High resolution MS data of molecular sphingolipid species in lipid extracts of investigated strains

Strain	Compound Name	Library RT (min)	Library MM (Da)	Chemical Formula	Chemical Formula Ion	Measured m/z	Calculated m/z	Error (ppm)
Wild-type	Cer(d19:0/16:0)	8.215	553.5434	C35H71NO3	C36H72NO5	598.5454	598.54160	−6.3
	Cer(d19:0/i17:0 2-OH)	8.034	583.554	C36H73NO4	C37H74NO6	628.5564	628.5522	−6.7
	Cer(d19:0/i17:0)	8.305	567.559	C36H73NO3	C37H74NO5	612.5618	612.5572	−7.4
	PI-Cer(d19:0/16:0 2-OH)	7.425	811.5575	C41H82NO12P	C41H81NO12P	810.5457	810.5502	5.5
	PI-Cer(d19:0/16:0)	7.614	795.5625	C41H82NO11P	C41H81NO11P	794.56106	794.55527	−7.3
	PI-Cer(d19:0/i17:0 2-OH)	7.549	825.5731	C42H84NO12P	C42H83NO12P	824.5644	824.5658	1.7
	PI-Cer(d19:0/i17:0)	7.729	809.5782	C42H84NO11P	C42H83NO11P	808.5691	808.5709	2.2
Δ0191	Cer(d19:0/16:0)	8.215	553.5434	C35H71NO3	C36H72NO5	598.5415	598.5416	0.1
	Cer(d19:0/i17:0)	8.305	567.559	C36H73NO3	C36H74NO5	612.5579	612.5572	−1.1
	PI-Cer(d19:0/16:0)	7.614	795.5625	C41H82NO11P	C41H81NO11P	794.5525	794.5553	3.5
	PI-Cer(d19:0/i17:0)	7.729	809.5782	C42H84NO11P	C42H83NO11P	808.5714	808.5709	−0.6
⁻MXAN_1528	Cer(d19:0/16:0)	8.215	553.5434	C35H71NO3	C36H72NO3	598.5434	598.5416	−3.1
	Cer(d19:0/i17:0 2-OH)	8.034	583.554	C36H73NO4	C37H74NO4	628.5552	628.5522	−4.9
	Cer(d19:0/i17:0)	8.305	567.559	C36H73NO3	C37H74NO3	612.5608	612.5572	−5.7
	PI-Cer(d19:0/16:0 2-OH)	7.425	811.5575	C41H82NO12P	C41H81NO12P	810.5503	810.5502	−0.1
	PI-Cer(d19:0/16:0)	7.614	795.5625	C41H82NO11P	C41H81NO11P	794.556	794.5553	−0.9
	PI-Cer(d19:0/i17:0 2-OH)	7.549	825.5731	C42H84NO12P	C42H83NO12P	824.5661	824.5658	−0.4
	PI-Cer(d19:0/i17:0)	7.729	809.5782	C42H84NO11P	C42H83NO11P	808.5714	808.5709	−0.6

RT, retention time; MM, molecular mass.

Analogously, in strain ⁻MXAN_1528 bearing a mutation in *elbD*, a multidomain enzyme involved in ether lipid biosynthesis (12), the relative abundance of vinyl ether species is strongly reduced (Table 2, Fig. 4C).

Lipid profiles of various mutants deficient in lipid biosynthesis

Integration of EIC peak areas of the monoisotopic masses of the respective lipid molecular species allows the construction of lipid profiles. If only the relative proportion of all lipid species are compared among the various investigated strains, no major differences are observable, apart from the above mentioned loss of certain lipid species and the expected relative increase of the remaining molecular species (supplementary Fig. VIII).

In order to gain an in-depth look into the lipid profile of *M. xanthus*, we constructed a scatter plot comprising mass, retention time, and relative abundances of all analyzed lipid molecular species given as the sum of all peak areas per thousand (**Fig. 5**; Table 1; supplementary Tables I, II). The observed pattern reflects previous results from GC-MS analysis of FAMEs and neutral lipids with a high proportion of lipid molecular species containing 15:0 and 16:1. The occurring FAs are somewhat equally distributed among the various lipid classes with an almost "Gaussian"-like distribution among the TGs and PEs (Fig. 5). Like Curtis et al. (11), we identified numerous PE and also PG molecular species with unsaturated FAs attached to the *sn*-1 position of the glycerol backbone (Table 1), indicating a less specific glycerol-3-phosphate 1-*O*-acyltransferase activity compared with *Escherichia coli*, where those lipids are less prevalent (32). Vinyl ether-containing phospholipids were exclusively detected within the PE molecules, whereas *O*-alkylglycerols could not be detected under these conditions, which is consistent with previous results (4). The relatively low proportion of PGs is consistent with results from Orndorff and Dworkin (15), who specified the amount of PGs as 9% of total $^{32}PO_4^{3-}$-labeled *M. xanthus* membranes. Analogously, CLs are minor compounds, but exhibit a high molecular diversity, as each molecule is potentially made up of four different FAs (Table 1). Neutral lipids, especially TGs, gave strong signals as ammonium adducts, although they are less prevalent in vegetative cells (10). Their molecular diversity seems to be even higher than that of the polar lipids.

In an additional step, we created scatter plots that compare the relative changes in the abundance of the individual lipid species between the mutant lipid profiles and the wild-type profile. This reflects the changes in the abundance of individual molecular species in the analyzed mutant strains compared with the wild-type, displayed in a 3D way. Now, shifts and trends in the mutant profiles are able to be visually appraised (**Fig. 6A–C**, supplementary Table I).

The lipid profile of strain Δ0191 versus wild-type shows the expected relative increase of nonhydroxylated Cers in addition to the aforementioned loss of hydroxylated Cer molecular species and a general increase in the abundance of PG molecular species (Fig. 6A, Table 1). There is a conspicuous increase in PE(15:0/17:0) and a simultaneous
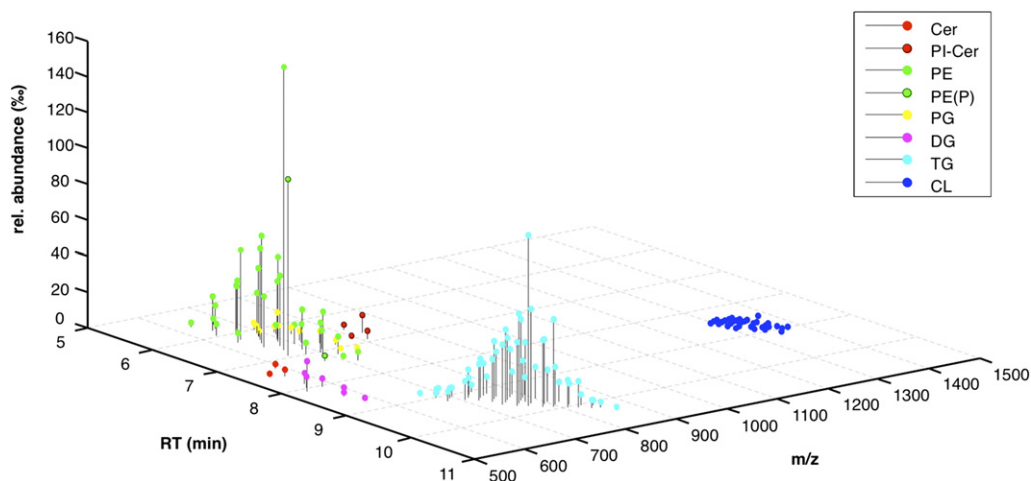
Fig. 5. Lipid profile of *M. xanthus* DK1622 wild-type. Data from Table 1 visualized in a scatter plot with relative abundance of individual lipid molecular species given as per thousand of the total abundance of all lipid species separately determined for the positive and negative ionization mode.

strong decrease in the abundance of PE(15:0/15:0) and PE(15:1/15:0). These findings match well with the FAME pattern of strain Δ0191, which shows a higher proportion of i17:0 FA compared with the wild-type (Table 2). The changes in abundance within the TG molecular species seem to be rather random, but could be attributed to a higher ratio of iso17:0 to iso15:0 FAs.

Figure 6B visualizes the changes in the lipid profile of ⁻MXAN_3748 compared with the wild-type. A general increase in higher molecular weight lipid species within the PE, PG, and TG molecular species, as well as a greater proportion of PE(P), is observable, meaning that there is a general increase in longer and/or less saturated FAs that could compensate for the loss of the lipophilic Cer species.

The scatter plot in Fig. 6C shows the expected decrease of PE(P-15:0/15:0) in the ⁻MXAN_1528 mutant. Rather surprising is the synchronous relative drop in PE(15:0/15:0) and TG(15:0/15:0/15:0), suggesting that all these lipid species share a common precursor.

DISCUSSION

Such a comprehensive data set about molecular lipid species in myxobacteria has not been published before. Curtis et al. (38) reported the analysis of lipid molecular species from the PE fraction of *M. xanthus* by HPLC-ESI-MS, resulting in the identification of 26 PE molecular species; though for four of these, no assignment of the fatty acyl residues to the *sn*-1 and *sn*-2 position of the glycerol backbone was achieved. Our UPLC-MS analysis confirmed that α-hydroxylation of FAs and sphingolipid formation are indeed metabolically linked, as the lipid extract of the α-hydroxylase deletion mutant Δ0191 lacks the hydroxylated sphingolipids and the *spt*-disruption mutant ⁻MXAN_3748 is devoid of any detectable sphingolipids and does not contain other lipids with an α-hydroxylated FA. When the results concerning the abundance of neutral lipids are compared with those obtained by high temperature GC-MS

analysis (10), it seems that the latter method results in overestimation of the presence of MGs and DGs. This is very likely due to the derivatization procedure with N-Methyl-N-(trimethylsilyl) trifluoroacetamide, which converts the free hydroxy groups of the MGs and DGs into easily ionizable trimethylsilyl derivates. In contrast, identical amounts of TGs yield more intense ESI-MS signals than underivatized MGs or DGs (Fig. 1). In the end, the creation of calibration curves using molecular standards for every lipid class will be necessary to determine their individual response factors. This will be the only way to establish the exact ratio between different lipid classes. Although not further evaluated, it is interesting that the TG molecular species seem to contain fatty acyl species that are not detectable in FAME-GC-MS analysis, as the [M-NH₃-RₙCOOH]⁺ fragment at m/z 521.6 in the mass spectrum shown in supplementary Fig. VIIC indicates the neutral loss of an 18:1 FA.

We did not detect any glycerophosphoserines or lysophospholipids during our analysis, although these molecules are putative precursors of the highly abundant PEs or their degradation products, respectively. These lipids were detected in ³²PO₄³⁻-labeled TLC-resolved membrane fractions of *M. xanthus*, but not in its whole cell lipid extract (15), leading us to conclude that they are products of ongoing enzymatic reactions during the lengthy membrane fractionation procedure. We cannot exclude the presence of traces of these compounds with abundances lower than the limit of detection. The use of a column with a higher resolution and different MS experiments and instrumentation may lead to the identification of more lipid species. However, trace component analysis was not the intention of this study.

At the same time, the low abundance of CLs, as determined by our ESI-MS analyses, is consistent with the low abundance of CLs found in the ³²PO₄³⁻-labeled cells (15).

The presence of PI-Cers is an interesting finding of this study, as this is a class of lipid known to be present in fungi such as *Saccharomyces cerevisiae* (39) and *Aspergillus niger*
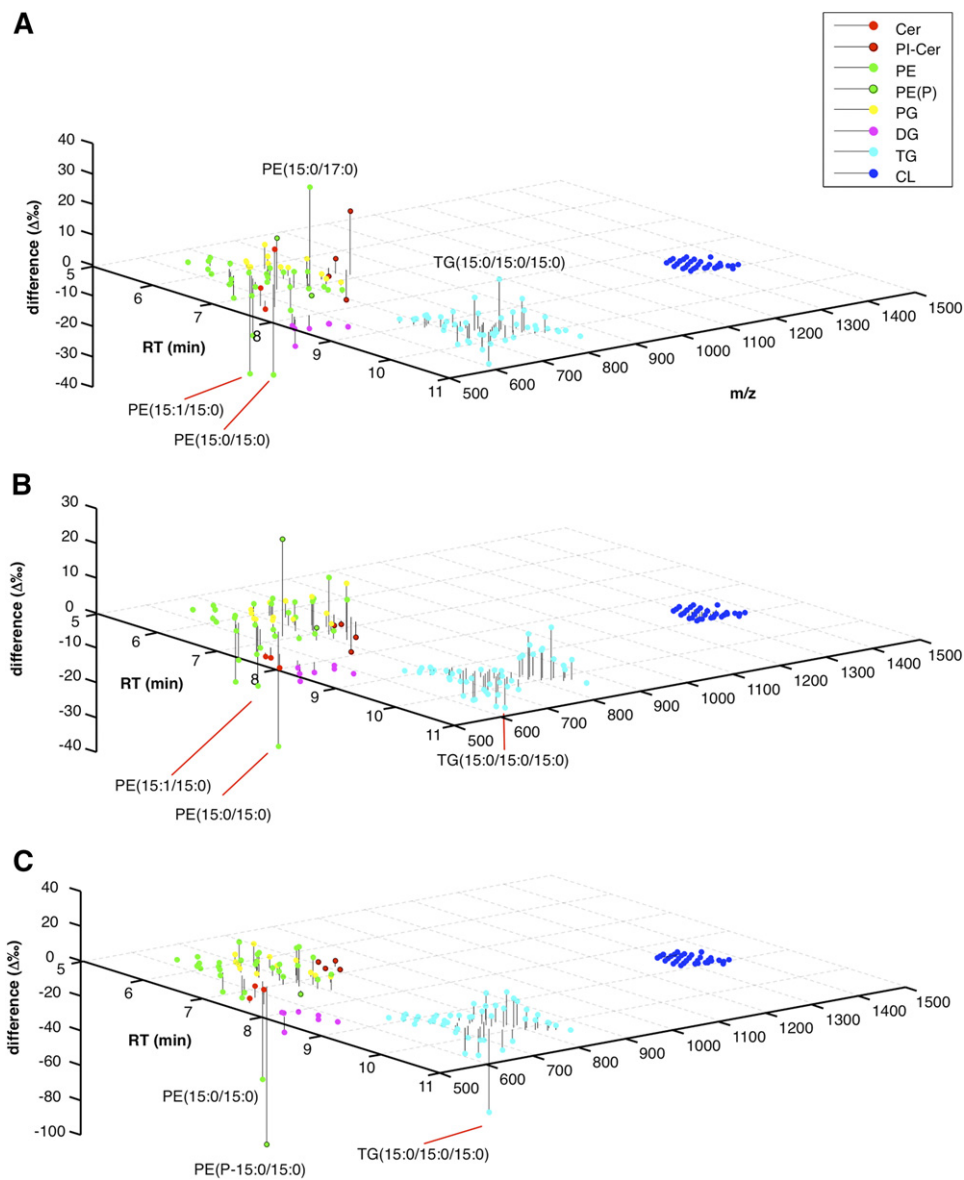
Fig. 6. Relative changes in the lipid profile of Δ0191 (A), ⁻MXAN_3748 (B), and ⁻MXAN_1528 (C) versus wild-type. For details see text.

(40). They have also been found in protozoan pathogens like *Trichomonas brucei* (41), *Trypanosoma brucei* (41), *Leishmania major* (42), and plants (43). However, to our knowledge, the occurrence of bacterial PI-Cers has never been previously described. It seems that sphingolipids are a common component of myxobacterial membranes, as Cers were found in *Cystobacter fuscus* (44), Cer phosphoethanolamines in *Myxococcus stipitatus* (45), and Cer phosphoethanolamines, β-D-glucosylsphingenines, and even phosphonosphingolipids in *Sorangium cellulosum* So ce56 (46), where they serve together with ornithine-containing lipids and glycerol ether lipids as substitutes for missing lipopolysaccharides in the outer membrane (46).

In *S. cerevisiae*, PI-Cers are synthesized by the inositol phosphorylceramide synthase catalytic subunit (AUR1), an enzyme that transfers a phosphoinositol headgroup to α-hydroxyceramides from a diacylglycerophosphoinositol

moiety (47). Protein MXAN_0451 (annotated as a PAP2 family protein) is 29% homologous to AUR1 (E-value = 2^{-20}), a further indication of the capability of *M. xanthus* to synthesize this lipid species. Interestingly, no diacylglycerophosphoinositols were detected in the lipid extracts, though it has been previously noted that a *myo*-inositol-1-phosphate synthase homolog (MXAN_0452) as well as a CDP-alcohol phosphatidyltransferase homolog (MXAN_0450) are encoded next to MXAN_0451 (48). This may be due to a fast conversion of diacylglycerophosphoinositols to PI-Cers as the occurrence of diacylglycerophosphoinositols are indeed described for *M. fulvus* and *S. aurantiaca* (13).

In general, glycosylated Cers are important signaling molecules in multicellular organisms (49), but no specific functions for PI-Cers are known in lower eukaryotes, except that inhibition of AUR1 is lethal to *S. cerevisiae* (50) and that PI-Cer is at least indirectly associated with the

pathogenicity of *Cryptococcus neoformans* (51). A possible signaling function of PI-Cers in myxobacterial fruiting body formation or sporulation remains to be investigated. Although there have been no systematic investigations on putative signaling functions of Cers in bacteria, it was noted that sphingolipids (as determined by the sphingobases) accumulate in developing *M. xanthus* cells, but are dispensable for fruiting body formation (9).

In summary, the changes in the lipid profiles between wild-type and mutant strains can be used to unveil genes and their protein products that are involved in lipid biosynthesis. An overview about gene candidates with homology to genes involved in lipid biosynthesis from other organisms exists in the literature (48). Even when there is functional redundancy between paralogous genes, it is possible to deduce protein functions from shifts in the lipid profiles of the respective mutant as shown in Fig. 6A for the Δ0191 mutant, in which the biosynthesis of a polar headgroup is not affected.

We are aware that final statements concerning changes in lipid profiles are not possible without statistically analyzable data, although some observable changes, like the previously established decrease or loss of selected molecular species and the easily explained general increase in degree of saturation and chain length of FAs within the lipids suggest that our data analysis procedure is generally a valid approach. Moreover, the visualization of the data using scatter plots resolved by the lipid class strongly facilitates data inspection and interpretation. This becomes even more important with increasing numbers of analytes. We envision that refinement of this method using appropriate internal standards and statistics will yield lipid profiles that can be linked to transition profiles, diffusibility of membranes, activities of selected membrane proteins and membrane proteomes, and allow us to unravel the multifactorial links between those properties and the lipid composition of membranes.

REFERENCES

1. Kaiser, D. 2008. *Myxococcus*—from single-cell polarity to complex multicellular patterns. *Annu. Rev. Genet.* **42:** 109–130.
2. Weissman, K. J., and R. Müller. 2010. Myxobacterial secondary metabolites: bioactivities and modes-of-action. *Nat. Prod. Rep.* **27:** 1276–1295.
3. Kearns, D. B., and L. J. Shimkets. 2001. Lipid chemotaxis and signal transduction in *Myxococcus xanthus. Trends Microbiol.* **9:** 126–129.
4. Ring, M. W., G. Schwär, V. Thiel, J. S. Dickschat, R. M. Kroppenstedt, S. Schulz, and H. B. Bode. 2006. Novel iso-branched ether lipids as specific markers of developmental sporulation in the myxobacterium *Myxococcus xanthus. J. Biol. Chem.* **281:** 36691–36700.
5. Bhat, S., T. Ahrendt, C. Dauth, H. B. Bode, and L. J. Shimkets. 2014. Two lipid signals guide fruiting body development of *Myxococcus xanthus. MBio.* **5:** e00939–e009313.
6. Fautz, E., G. Rosenfelder, and L. Grotjahn. 1979. Iso-branched 2- and 3-hydroxy fatty acids as characteristic lipid constituents of some gliding bacteria. *J. Bacteriol.* **140:** 852–858.
7. Bode, H. B., M. W. Ring, D. Kaiser, A. C. David, R. M. Kroppenstedt, and G. Schwär. 2006. Straight-chain fatty acids are dispensable in the myxobacterium *Myxococcus xanthus* for vegetative growth and fruiting body formation. *J. Bacteriol.* **188:** 5632–5634.
8. Ring, M. W., E. Bode, G. Schwär, and H. B. Bode. 2009. Functional analysis of desaturases from the myxobacterium *Myxococcus xanthus. FEMS Microbiol. Lett.* **296:** 124–130.
9. Ring, M. W., G. Schwär, and H. B. Bode. 2009. Biosynthesis of 2-hydroxy and iso-even fatty acids is connected to sphingolipid formation in myxobacteria. *ChemBioChem.* **10:** 2003–2010.
10. Hoiczyk, E., M. W. Ring, C. A. McHugh, G. Schwär, E. Bode, D. Krug, M. O. Altmeyer, J. Z. Lu, and H. B. Bode. 2009. Lipid body formation plays a central role in cell fate determination during developmental differentiation of *Myxococcus xanthus. Mol. Microbiol.* **74:** 497–517.
11. Curtis, P. D., R. Geyer, D. C. White, and L. J. Shimkets. 2006. Novel lipids in *Myxococcus xanthus* and their role in chemotaxis. *Environ. Microbiol.* **8:** 1935–1949.
12. Lorenzen, W., T. Ahrendt, K. A. J. Bozhüyük, and H. B. Bode. 2014. A multifunctional enzyme is involved in bacterial ether lipid biosynthesis. *Nat. Chem. Biol.* **10:** 425–427.
13. Caillon, E., B. Lubochinsky, and D. Rigomier. 1983. Occurrence of dialkyl ether phospholipids in *Stigmatella aurantiaca* DW4. *J. Bacteriol.* **153:** 1348–1351.
14. Kleinig, H. 1972. Membranes from *Myxococcus fulvus* (Myxobacterales) containing carotenoid glucosides. I. Isolation and composition. *Biochim. Biophys. Acta.* **274:** 489–498.
15. Orndorff, P. E., and M. Dworkin. 1980. Separation and properties of the cytoplasmic and outer membranes of vegetative cells of *Myxococcus xanthus. J. Bacteriol.* **141:** 914–927.
16. Fuchs, B., and J. Schiller. 2009. Application of MALDI-TOF mass spectrometry in lipidomics. *Eur. J. Lipid Sci. Technol.* **111:** 83–98.
17. Han, X., K. Yang, and R. W. Gross. 2012. Multi-dimensional mass spectrometry-based shotgun lipidomics and novel strategies for lipidomic analyses. *Mass Spectrom. Rev.* **31:** 134–178.
18. Furey, A., M. Moriarty, V. Bane, B. Kinsella, and M. Lehane. 2013. Ion suppression; a critical review on causes, evaluation, prevention and applications. *Talanta.* **115:** 104–122.
19. Shan, L., K. Jaffe, S. Li, and L. Davis. 2008. Quantitative determination of lysophosphatidic acid by LC/ESI/MS/MS employing a reversed phase HPLC column. *J. Chromatogr. B Analyt. Technol. Biomed. Life Sci.* **864:** 22–28.
20. Hutchins, P. M., R. M. Barkley, and R. C. Murphy. 2008. Separation of cellular nonpolar neutral lipids by normal-phase chromatography and analysis by electrospray ionization mass spectrometry. *J. Lipid Res.* **49:** 804–813.
21. Rütters, H., H. Sass, H. Cypionka, and J. Rullkötter. 2001. Monoalkylether phospholipids in the sulfate-reducing bacteria *Desulfosarcina variabilis* and *Desulforhabdus amnigenus. Arch. Microbiol.* **176:** 435–442.
22. Bligh, E. G., and W. J. Dyer. 1959. A rapid method of total lipid extraction and purification. *Can. J. Biochem. Physiol.* **37:** 911–917.
23. Bode, H. B., M. W. Ring, G. Schwär, R. M. Kroppenstedt, D. Kaiser, and R. Müller. 2006. 3-Hydroxy-3-methylglutaryl-coenzyme A (CoA) synthase is involved in biosynthesis of isovaleryl-CoA in the myxobacterium *Myxococcus xanthus* during fruiting body formation. *J. Bacteriol.* **188:** 6524–6528.
24. Lipid Maps: Lipidomics Gateway. Accessed 26 September 2014 at http://www.lipidmaps.org.
25. Ejsing, C. S. 2007. Molecular Characterization of the Lipidome by Mass Spectrometry. Doctoral Thesis. Technische Universität Dresden, Dresden, Germany.
26. Blaas, N., and H. Humpf. 2013. Structural profiling and quantitation of glycosyl inositol phosphoceramides in plants with Fourier transform mass spectrometry. *J. Agric. Food Chem.* **61:** 4257–4269.
27. Elkhayat, E. S., G. A. Mohamed, and S. R. M. Ibrahim. 2012. Activity and structure elucidation of ceramides. *Curr. Bioact. Compd.* **8:** 370–409.
28. Scherer, M., G. Schmitz, and G. Liebisch. 2010. Simultaneous quantification of cardiolipin, bis(monoacylglycero)phosphate and their precursors by hydrophilic interaction LC-MS/MS including correction of isotopic overlap. *Anal. Chem.* **82:** 8794–8799.
29. Zemski Berry, K. A., and R. C. Murphy. 2004. Electrospray ionization tandem mass spectrometry of glycerophosphoethanolamine plasmalogen phospholipids. *J. Am. Soc. Mass Spectrom.* **15:** 1499–1508.
30. Hsu, F. F., J. Turk, E. R. Rhoades, D. G. Russell, Y. Shi, and E. A. Groisman. 2005. Structural characterization of cardiolipin by tandem quadrupole and multiple-stage quadrupole ion-trap mass

spectrometry with electrospray ionization. *J. Am. Soc. Mass Spectrom.* **16:** 491–504.

31. Smith, P. B., A. P. Snyder, and C. S. Harden. 1995. Characterization of bacterial phospholipids by electrospray ionization tandem mass spectrometry. *Anal. Chem.* **67:** 1824–1830.

32. Oursel, D., C. Loutelier-Bourhis, N. Orange, S. Chevalier, V. Norris, and C. M. Lange. 2007. Lipid composition of membranes of *Escherichia coli* by liquid chromatography/tandem mass spectrometry using negative electrospray ionization. *Rapid Commun. Mass Spectrom.* **21:** 1721–1728.

33. Murphy, R. C., P. F. James, A. M. McAnoy, J. Krank, E. Duchoslav, and R. M. Barkley. 2007. Detection of the abundance of diacylglycerol and triacylglycerol molecular species in cells using neutral loss mass spectrometry. *Anal. Biochem.* **366:** 59–70.

34. Tsui, F. C., D. M. Ojcius, and W. L. Hubbell. 1986. The intrinsic pKa values for phosphatidylserine and phosphatidylethanolamine in phosphatidylcholine host bilayers. *Biophys. J.* **49:** 459–468.

35. Marsh, D. 1990. CRC Handbook of Lipid Bilayers. CRC Press, Boca Raton, FL.

36. Kaiser, D. 1979. Social gliding is correlated with the presence of pili in *Myxococcus xanthus. Proc. Natl. Acad. Sci. USA.* **76:** 5952–5956.

37. Murphy, R. C., and P. H. Axelsen. 2011. Mass spectrometric analysis of long-chain lipids. *Mass Spectrom. Rev.* **30:** 579–599.

38. Curtis, P. D., R. Geyer, D. C. White, and L. J. Shimkets. 2006. Novel lipids in *Myxococcus xanthus* and their role in chemotaxis. *Environ. Microbiol.* **8:** 1935–1949.

39. Becker, G. W., and R. L. Lester. 1980. Biosynthesis of phosphoinositol-containing sphingolipids from phosphatidylinositol by a membrane preparation from *Saccharomyces cerevisiae. J. Bacteriol.* **142:** 747–754.

40. Hackett, J. A., and P. J. Brennan. 1977. The isolation and biosynthesis of the ceramide-phosphoinositol of *Aspergillus niger. FEBS Lett.* **74:** 259–263.

41. Smith, T. K., and P. Bütikofer. 2010. Lipid metabolism in *Trypanosoma brucei. Mol. Biochem. Parasitol.* **172:** 66–79.

42. Hsu, F. F., J. Turk, K. Zhang, and S. M. Beverley. 2007. Characterization of inositol phosphorylceramides from *Leishmania major* by tandem mass spectrometry with electrospray ionization. *J. Am. Soc. Mass Spectrom.* **18:** 1591–1604.

43. Kaul, K., and R. L. Lester. 1975. Characterization of inositol-containing phosphosphingolipids from tobacco leaves: isolation and identification of two novel, major lipids: N-acetylglucosamidoglucuronidoinositol phosphorylceramide and glucosamidoglucuronidoinositol phosphorylceramide. *Plant Physiol.* **55:** 120–129.

44. Eckau, H., D. Dill, and H. Budzikiewicz. 1984. Neuartige ceramide aus *Cystobacter fuscus* (Myxobacterales). *Z. Naturforsch. C.* **39:** 1–9.

45. Stein, J., and H. Budzikiewicz. 1988. Ceramid-1-phosphoethanolamine aus *Myxococcus stipitatus. Z. Naturforsch. B.* **43:** 1063–1067.

46. Keck, M., N. Gisch, H. Moll, F. Vorhölter, K. Gerth, U. Kahmann, M. Lissel, B. Lindner, K. Niehaus, and O. Holst. 2011. Unusual outer membrane lipid composition of the gram-negative, lipopolysaccharide-lacking myxobacterium *Sorangium cellulosum* So ce56. *J. Biol. Chem.* **286:** 12850–12859.

47. Levine, T. P., C. A. Wiggins, and S. Munro. 2000. Inositol phosphorylceramide synthase is located in the Golgi apparatus of *Saccharomyces cerevisiae. Mol. Biol. Cell.* **11:** 2267–2281.

48. Curtis, P. D., and L. J. Shimkets. Chapter IV: Structure and Metabolism (subchapter) *In* Myxobacteria: Multicellularity and Differentiation. D. E. Whitworth, editor. ASM Press, Washington, DC. 248–258.

49. Buré, C., J. Cacas, S. Mongrand, and J. Schmitter. 2014. Characterization of glycosyl inositol phosphoryl ceramides from plants and fungi by mass spectrometry. *Anal. Bioanal. Chem.* **406:** 995–1010.

50. Zhong, W., M. W. Jeffries, and N. H. Georgopapadakou. 2000. Inhibition of inositol phosphorylceramide synthase by aureobasidin A in *Candida* and *Aspergillus* species. *Antimicrob. Agents Chemother.* **44:** 651–653.

51. Rhome, R., M. D. del Poeta, and M. del Poeta. 2009. Lipid signaling in pathogenic fungi. *Annu. Rev. Microbiol.* **63:** 119–131.